Optical-Pumping Determination of the Nuclear Magnetic Moments of the Radioisotopes Mercury-193, -193m, -195m, and -197m†

P. A. Moskowitz,* C. H. Liu,‡ G. Fulop, and H. H. Stroke
Department of Physics, New York University, Bronx, New York 10453

(Received 26 March 1971)

The technique of optical pumping has been used to determine the nuclear magnetic dipole moment of spin-$\frac{3}{2}$, 4-h ^{193}Hg, and the spin-$\frac{13}{2}$ isomers, 10-h ^{193m}Hg, 40-h ^{195m}Hg, and 24-h ^{197m}Hg. Nuclear magnetic resonance was observed following orientation of the $6s^2\ ^1S_0$ ground state. The results are $|^{193}\mu| = 0.617\,63(18)\mu_N$, $|^{193m}\mu| = 1.0416(3)\mu_N$, $|^{195m}\mu| = 1.0280(2)\mu_N$, and $|^{197m}\mu| = 1.0112(3)\mu_N$, all without diamagnetic correction. Differential hfs anomalies, Δ, have been calculated with respect to stable ^{199}Hg with the use of the previously determined values of the magnetic dipole hfs interaction constants for the $6s6p\ ^3P_1$ level. We obtain $^{193}\Delta^{199} = 0.0054(27)$, $^{193m}\Delta^{199} = 0.0108(3)$, $^{195m}\Delta^{199} = 0.0106(2)$, and $^{197m}\Delta^{199} = 0.0105(6)$.

I. INTRODUCTION

In a continuing program of systematic studies of nuclear charge and magnetization structures through their influence on atomic hfs,[1] we have made direct measurements by the technique of optical pumping of the nuclear magnetic moments of 4-h ^{193}Hg, and of the spin-$\frac{13}{2}$ isomers 10-h ^{193m}Hg, 40-h ^{195m}Hg, and 24-h ^{197m}Hg. It is the first time that orientation of such high-spin nuclei has been achieved.[2] ^{193}Hg is the shortest-lived mercury isotope for which a precision measurement of the nuclear magnetic moment has been made. It thus brings to nine the number of such isotopes and nuclear isomers of mercury for which we can also determine the effects of the distribution of the nuclear magnetization – the hfs anomalies.[3] Because mercury is a heavy element, nuclear-structure effects are expected to be important. It is therefore fortunate that the range of isotopes that we can study systematically at present (i.e., with a limit of a half-life of a few h for the radioisotopes and isomers) extends from mass number 192 to 204. We can perform precise optical experiments with isotopic samples in quantities of the order of 1 ng. In all these we use the strong $6s6p\ ^3P_1$-$6s^2\ ^1S_0$ 2537-Å resonance radiation for excitation.

Optical-magnetic-resonance experimentation has been developed extensively since its inception by Fermi and Rasetti.[4-15] Of particular importance to us here is the optical-pumping technique used by Bell and Bloom.[13] It is described in Sec. III C. We made use of a modification of their technique (Sec. III) in the present measurements.

II. HFS AND NUCLEAR STRUCTURE

We summarize features of the hfs interaction[16] between the atomic electrons and the nucleus relevant to our experiment. The result is usually given in terms of perturbation energies W that arise from the various terms of a multipole expansion of the hfs interaction. Because of parity restrictions, the nonvanishing multipoles have odd orders k for the magnetic interactions, and even orders for the electric interaction. The values of k are limited further by a maximum equal to the smaller of $2I$ or $2J$, where I and J are, respectively, the total nuclear and electronic angular-momentum quantum numbers. Since in our experiments the maximum J value involved is 1, we are thus limited to $k \leq 2$. The total angular momentum of the system is characterized by $F = I + J$. To first order we also have[17] $\sum(2F+1)W_F(k) = 0$, for all $k \neq 0$. This theorem for the hfs multiplet implies that the multipole interactions do not shift the center of gravity of the fine-structure levels. The monopole part of the electron-nuclear interaction that results from the nonpunctual nuclear charge distribution is, however, observable in the spectroscopic isotope shift. We discussed previously[18] many of the experimental data pertaining to this work. Here we are concerned primarily with the effect of the extended nuclear magnetization on the hfs interaction, i.e., on the evaluation of the magnetic dipole term of the Hamiltonian $A\vec{I}\cdot\vec{J}$. Electrons that penetrate the nucleus can thus serve to study its electric and magnetic structure.

The magnetic dipole interaction constant A is proportional to the magnetic field produced at the nucleus by the atomic electrons, and to the nuclear magnetization. For a point nucleus this is taken to be proportional to the nuclear g value. We can write for the actual nucleus

$$A = A(\text{point})(1+\epsilon)\ , \qquad \text{(II.1)}$$

which defines the hfs anomaly ϵ.[3] It accounts for the nonpunctual nuclear-structure influence on the

hfs. A is the measured hfs interaction constant; A(point) is the value that it would have for a puntual nucleus. [For alkalis, for example, $A(\text{point}) = \frac{16}{3}\pi g\mu_0{}^2\psi^2(0)$; μ_0 is the Bohr magneton and $\psi^2(0)$ is the probability of electrons to be at the position of the nucleus.] The latter value, however, is generally not calculable with sufficient accuracy to allow the determination of ϵ from (II.1), because of lack of precise knowledge of the corresponding electron wave functions. Instead, we study two isotopes and form the ratio

$$\frac{A_1}{A_2} = \frac{A_1(\text{point})(1+\epsilon_1)}{A_2(\text{point})(1+\epsilon_2)} \tag{II.2}$$

in which we use then

$$\frac{A_1(\text{point})}{A_2(\text{point})} \approx \frac{g_1}{g_2} . \tag{II.3}$$

If we neglect the relatively small effect of the difference in the distortions of the atomic wave functions caused by the extended nuclear charge distribution in the two isotopes,[19] we can take an equal sign in (II.3). For atomic electrons, the values of ϵ rarely exceed a few percent.[20] Therefore we can combine (II.2) and (II.3) to obtain the differential hfs anomaly

$${}^1\Delta^2 = \frac{A_1 g_2}{A_2 g_1} - 1 \approx \epsilon_1 - \epsilon_2 . \tag{II.4}$$

The determination of Δ depends on the measurements of the magnetic dipole hfs interaction constants and, independently, of the nuclear g values of the isotope pairs. A nonzero value of Δ results from the fact that in hfs the nuclear dipole magnetization interacts with the slightly inhomogeneous magnetic field caused by electrons, while in NMR it interacts with a homogeneous external field. The present optical-pumping measurements of the g values of the several radioisotopes of mercury allow the determination of differential hfs anomalies, since the A values have been measured previously. Finally, we point out that in the case of muonic atoms the muon wave function is known sufficiently well in order to determine ϵ directly from (II.1).[21] In heavy elements it is found to be of the order of 50%. As in isotope-shift studies, the muonic and electronic measurements of the hfs anomalies should prove to be complementary.

III. OPTICAL PUMPING

A. Orientation

The observation of NMR requires, in our case, a population difference among the ground-state magnetic sublevels, m, of the odd-N mercury isotopes. At room temperature, and in a magnetic field $\approx$1 G, the Boltzmann distribution produces only a negligible difference. Optical pumping, on the other hand, can achieve substantial population differences. We recall first the principle of the basic process and then that of the detection technique used in our experiments.

Figure 1 shows the magnetic-field hfs of an atom with a diamagnetic ${}^1S_0$ ground state, nuclear spin $I = \frac{3}{2}$ (as is the case for ^{201}Hg or ^{193}Hg), connected by resonance radiation to an excited ${}^3P_1$, $F = \frac{5}{2}$ level. If the atoms are excited with σ^+ circularly polarized light, taking account of the indicated relative transition probabilities, it can be seen that the repopulation of ground-state atoms is such that the higher-m states (ideally only the $m_F = \frac{3}{2}$ state) become filled preferentially. The atoms are thus "oriented" and the transparency of the atomic vapor to the σ^+ exciting radiation changes as time progresses.

B. Relaxation

Competing with the optical-pumping orientation are disorienting relaxation processes.[14] These are caused, in general, by collisions with the walls, other atoms in the vapor, and recondensation. In our experiments the atom density was so low that only wall effects are expected to be of importance. Cagnac found that the relaxation rate was not determined by the collision frequency, as given by the resonance-cell dimension and temperature, but by the dwell time on the wall. For ^{199}Hg, for example, the relaxation time was found to increase rapidly above a temperature $T \approx 100$°C. This result is consistent both with our earlier finding[22] that mercury atoms do not stick to the quartz walls above this temperature, and with our present experiment (Sec. IV A 3). The relaxation rate was also found by Cagnac to be much longer for ^{199}Hg ($I = \frac{1}{2}$), which has only a nuclear magnetic dipole moment, than for ^{201}Hg ($I = \frac{3}{2}$), which also

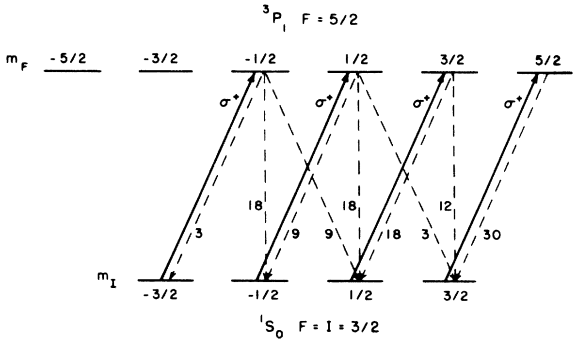

FIG. 1. Zeeman splitting of $J=0$, $F=I=\frac{3}{2}$ and $J=1$, $F=\frac{5}{2}$ energy levels, appropriate to ^{193}Hg. The numbers next to the arrows indicate relative transition probabilities.

has an electric quadrupole moment, Q. The latter can interact relatively strongly with electric field gradients near the wall, and thereby cause disorientation. All isotopes studied in the present experiment have $I > \frac{1}{2}$, and $Q \neq 0$.

C. Nuclear Magnetic Resonance

The equilibrium population established in the optical-pumping process can be altered by the application of rf power at the frequency that corresponds to NMR, i.e., $g_I \mu_B H_0$, where H_0 is the externally applied static magnetic field, and g_I is the nuclear gyromagnetic ratio. The resonance condition can be observed as a change in intensity of the pumping beam, or of the side-scattered light that results from the redistribution of atoms among the magnetic sublevels. This technique was used by Walter[15] for ^{197}Hg, and by Walter and Stavn[23] for ^{195}Hg. Both of these radioactive isotopes have $I = \frac{1}{2}$. Attempts to observe NMR in their $I = \frac{13}{2}$ nuclear isomers were unsuccessful.

The resonance can also be detected as a modulation, at the NMR frequency, produced on a light beam transverse to the pumping beam.[12,13] The superior signal-to-noise ratio gained by this method was shown by Cohen-Tannoudji.[24] Further advantages were reviewed more recently by Kastler.[25]

We have used previously a modification of this technique to measure the magnetic moment of radioactive ^{203}Hg that has $I = \frac{5}{2}$.[26] Instead of two light beams, we use a single one, directed at 45° to H_0, that serves both for pumping and for monitoring. Carver and Partridge[27] show, with the use of the density-matrix description, that the signal S in an experiment of the type of Bell and Bloom[13] has the form

$$S = K(\chi' \cos\omega t + \chi'' \sin\omega t), \qquad \text{(III.1)}$$

where K is a constant. The rf field H_1 is directed perpendicularly to H_0 and has a frequency ω. The resonant frequency is $\omega_0 = \gamma H_0$, where γ is the gyromagnetic ratio in units of frequency per unit magnetic field. Γ is an appropriate damping constant that accounts for relaxations. In terms of the above definitions, we have

$$\chi' = \frac{(-\gamma H_1)(\omega_0 - \omega)}{\Gamma^2 + (\omega_0 - \omega)^2 + (\gamma H_1)^2}, \qquad \chi'' = \frac{(-\gamma H_1)\Gamma}{\Gamma^2 + (\omega_0 - \omega)^2 + (\gamma H_1)^2}, \qquad \text{(III.2)}$$

and hence S has dispersion- and Lorentz-shaped parts, 90° out of phase. By suitable adjustments of the phase of the phase-sensitive detector, it was possible in our experiments to observe either of these two signal shapes, or a mixture of both. We show in Appenoix I that the same signal shape is obtained with our modified technique, but with a reduction of signal strength.

D. Lamp Shifts

Cohen-Tannoudji[24] observed, and explained theoretically, small shifts in the NMR frequency (<1 Hz) when the wavelength of the pumping light does not coincide with that of the resonance radiation. The shift is found to be proportional to the light intensity, and is in opposite directions for σ^+ and σ^- light. For resonance radiation, a broadening of the signal is expected. We did not observe these effects, within experimental error, probably because of lower light intensity.

IV. EXPERIMENT

A. Apparatus

Figure 2 shows a schematic of the optical-pumping experiment. The sources of resonance radiation for illuminating the different isotope studied varied. They are described in Sec. 1, below. The pumping light was circularly polarized with the use of a linear polarizer (type PL-40, Polacoat, Blue Ash, Ohio), followed by a quarter-wave plate (Valpey-Fisher, Holliston, Massachusetts). A fused-quartz lens was used so that the entire resonance cell intercepted the pumping light. A 2537-Å interference filter (Infrared Industries, Thin Film Division, Cambridge, Massachusetts) which allows 25% transmission, was placed in front of the RCA 1P28 photomultiplier tube. We also used a newer, lower-noise version of the tube, type 1P28/V1.

The entire optical system was oriented at an angle of 45° to the axis of the field coils, as shown. Although, as was discussed in Sec. III C, the use of a single beam in this manner should degrade the signal quality, comparisons between this method and the cross-beam arrangement of Bell and Bloom[13] did not reveal a noticeable difference in the signal-to-noise ratio. The use of a single beam also made optical alignment easier.

The magnetic field at the position of the H_0 cell,

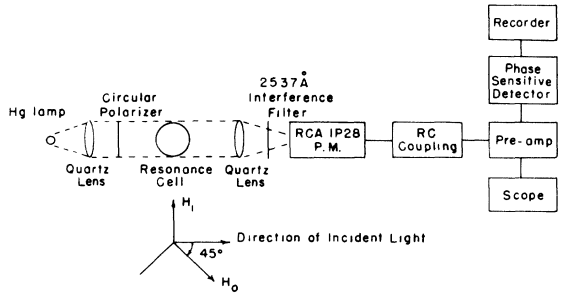

FIG. 2. Schematic diagram of the apparatus.

was produced by a pair of coils, each consisting of 200 turns of No. 22 copper wire. The coils had a diameter of 71 cm and were spaced 39 cm apart. They were aligned to make H_0 coaxial with the horizontal component of the magnetic field of the earth. Values of H_0, used in the experiment, ranged from 2 to 5 G. The current to the coils was supplied from a transistorized power supply (model No. 36100R, Power Designs Inc., Westbury, New York), and was controlled to within 3 parts in 10^5 by means of a circuit which monitored the current through a standard resistance in series with the coils. The magnetic field was swept over a range of approximately 100 mG in the vicinity of resonance while the frequency of the oscillating magnetic field H_1 was held constant. The ramp voltage for the sweep was obtained from a signal averager (Fabri-Tek, model 1074) which was also used to accumulate, store, and average the data.

The oscillating field was produced with the use of a pair of coils, placed so that H_1 was directed at right angles to the plane that contained H_0 and the light beam. The oscillator (General Radio, 1312 Decade Oscillator) maintained the frequency constant to within 1 part in 10^5. The maximum frequency used was 4100 Hz.

We made use of narrow-band amplification in the detection system in order to increase the signal-to-noise ratio. The output signal from the photomultiplier tube was impressed on a preamplifier (model 103, Keithley Corporation, Cleveland, Ohio), with a gain of 100, through a simple RC coupling circuit. This served to separate the resonance-frequency modulation of the transmitted light beam from dc variations of the light intensity.

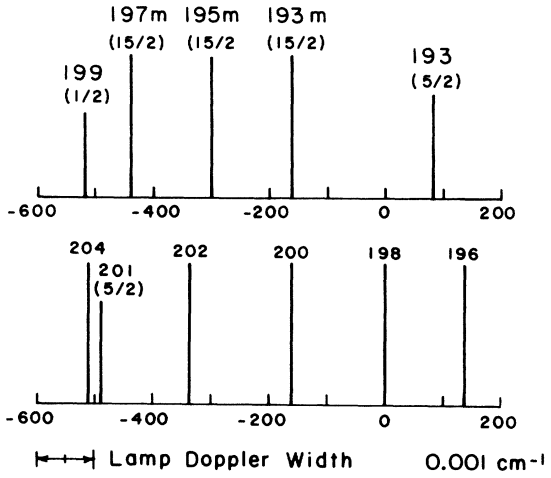

FIG. 3. Spectrum of the zero-field hfs components of the 2537-Å resonance line of mercury isotopes involved in the experiment. The components shown in the upper set were pumped by matching components in the lower set. ^{193}Hg was pumped by Zeeman-tuning the ^{193}Hg line. Units are in 0.001 cm^{-1}.

The resulting signal was detected with the use of a lock-in detector. (Princeton Applied Research, model HR 8) tuned to the resonance frequency. The output signal was then processed by the signal averager. An oscilloscope was also used to monitor the output of the audio amplifier. Often, the signal strength was sufficient to be observable directly on the oscilloscope.

In the case of very weak signals, the use of the signal averager improved substantially the signal-to-noise ratio. After the first cell (of a total of five), which was poorly produced, the maximum number of sweeps required was four. The stored data of the signal averager was recorded with the use of an X-Y recorder for analysis.

1. *Light Sources*

The wavelength of the exciting light used for optically pumping an isotope must correspond to that of the resonance transition from the $^1S_0$ ground state to a hyperfine level of an excited state (in our case $6s6p\ ^3P_1$). The relative wave numbers of the hfs components of the various radioactive isotopes studied are shown in Fig. 3, together with the positions of the appropriate stable mercury components. Because the full Doppler width at half-maximum intensity of the light emitted was about 70 mK (1 mK = 0.001 cm^{-1}), it can be seen that lamps made of stable isotopes could be used to excite the atoms of the three isomeric nuclei. In particular, the $F = \frac{5}{2}$ component of ^{201}Hg was used to excite ^{197m}Hg ($F = \frac{15}{2}$), ^{202}Hg excited ^{195m}Hg ($F = \frac{15}{2}$), and ^{200}Hg excited ^{193m}Hg ($F = \frac{15}{2}$). Table I shows the enrichments of the various isotopes of mercury that we obtained from Union Carbide Corporation, Oak Ridge, Tennessee.

In the case of ^{193}Hg, the $F = \frac{5}{2}$ component lies 54 mK from the ^{196}Hg line position. Therefore, the excitation frequency would lie in the wings of the lamp line shape. However, as indicated in Table I, the maximum enrichment of ^{196}Hg available for the construction of a lamp is only 48.2%. We constructed a ^{196}Hg lamp, but poor signal quality resulted with its use. Therefore, we resorted to a magnetic-scanning technique. A ^{198}Hg lamp was placed in a magnetic field of 1200 G, in an apparatus actually set up for an optical-pumping mag-

TABLE I. Enrichment of mercury isotopes used in our experiments.

Isotope	196	198	199	200	201	202	204
Enrichment (%)	48.2	94.4	86.1	88.9	81.5	92.8	84.0

netic-scanning experiment.[28] In this field, one of the three Zeeman components that resulted from the splitting of the $^3P_1$ line overlapped the ^{193}Hg, $F=\frac{5}{2}$ component. This excitation procedure yielded satisfactory results. The $F=\frac{1}{2}$ hfs component of ^{199}Hg, that served as the magnetic field calibrating isotope, was excited with the use of a ^{204}Hg lamp.

The lamps[29] consisted of a 1-cm-diam fused-quartz bulb filled with approximately 1 mg enriched mercury isotope and argon at a pressure of 2 Torr. The small electrodeless lamps were excited with the use of a one-transitor 100-MHz oscillator. The power drawn by the oscillator was less than 3 W. The lamps, when cooled by a stream of cool air, yielded an intense 2537-Å line almost free of self-reversal.

A $QK=61$ magnetron microwave oscillator was used to excite the ^{198}Hg lamp in the magnet in the ^{193}Hg orientation experiment. The extremely low noise level of the 100-MHz oscillator, its chief advantage, was sacrificed, but the light intensity was maintained.

2. *Isotope Production*

The radioactive isotopes were produced by the ^{197}Au$(p, xn)^{198-x}$Hg reaction (x is the number of neutrons ejected) with the use of the Harvard University cyclotron. At first, we selected the bombarding energy as we had done earlier,[18] i.e., based on the Bi and Pb excitation functions. For the $(p, 5n)$ reaction this was 55 MeV. Subsequently, we learned of the excitation studies with mercury by Poffé *et al.*[30] These showed that the peak of the production cross section ($\approx 2b$) was actually at 60 MeV. Five bombardments were thus made between 55 and 62 MeV. We found that it was possible to produce simultaneously adequate quantities of ^{193}Hg, ^{193m}Hg, ^{195m}Hg, and ^{197m}Hg. Poffé[31] observed that the ^{195m}Hg production was favored over that of ^{195}Hg in the ground state, especially at the lower proton-beam energies. We observed a similar favoring of the ^{193m}Hg production over that of ^{193}Hg.

The gold target foil ≈ 0.25 mm thick, 25×35 mm, was mounted on the internal probe of the cyclotron. 10- to 12-h bombardments, with a beam current 1 μA, produced approximately 10^{14} atoms of ^{193}Hg and ^{193m}Hg. The numbers of ^{195m}Hg and ^{197m}Hg atoms were lower by 1 and 2 orders of magnitude, respectively.

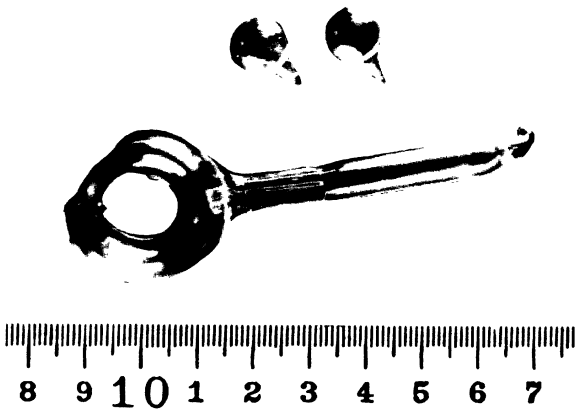

FIG. 4. Photograph of optical-pumping cell, and of spherical electrodeless lamps.

3. *Optical-Pumping Cell and Relaxation*

The cell was blown from fused quartz to a sphere, approximately 2.5 cm diam. A capillary filling tube joined the base of the cell, as shown in Fig. 4. The procedure for filling the cell with the radioactive isotopes is similar to the one that we used in making lamps,[18] except that here no carrier gas was used: The cyclotron target gold foil was melted under vacuum, with the use of an induction heater, to liberate the radioactive mercury. This was caught on clean gold foil in a first U trap, usually cooled with liquid nitrogen, from where the mercury was distilled into the cell. In the past, the last step risked either the loss of mercury into a second cold trap of the vacuum system, if pumping was allowed during the distillation, or the production of a dirty cell, if the cell-catcher-gold section was first pulled off from the vacuum system with the use of a flame. The heat at this step frequently liberated sufficient impurities to prevent the subsequent observation of the optical-pumping signal. A major improvement in the procedure was the use of a magnetically actuated ground-glass ball valve,[32] instead of the flame pull-off, to isolate the cell from the vacuum system before the final distillation of the mercury into the cell.

In addition to the radioactive mercury isotopes, $\approx 5\times 10^{13}$ ^{199}Hg atoms, which served for magnetic field calibration, were introduced into the cell. A small reservoir was prepared at a known vapor

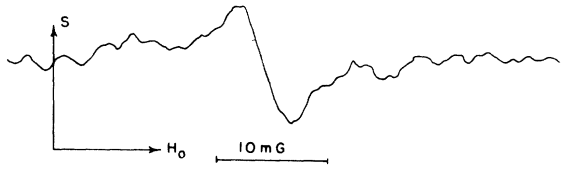

FIG. 5. ^{197m}Hg resonance signal. The phase of the lock-in amplifier was adjusted to detect the χ' part of the signal S [Eq. III. 1].

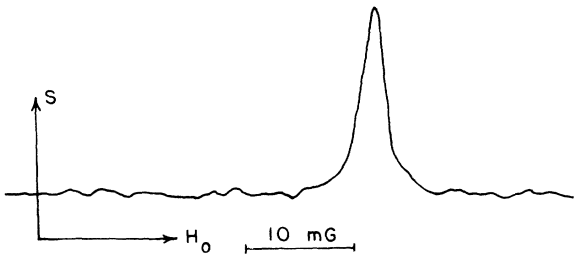

FIG. 6. ^{195m}Hg resonance signal. The phase of the lock-in amplifier was appropriate for the detection of the χ'' part of the signal S [Eq. (III.1)].

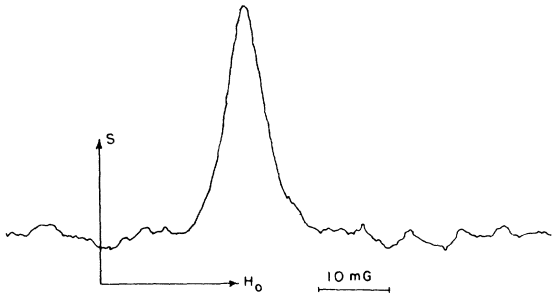

FIG. 7. ^{193}Hg resonance signal.

pressure with ^{199}Hg obtained by dissociating the mercury oxide. The ^{199}Hg was admitted to the cell manifold with the use of a break-off seal.

As we discussed in Sec. III B, relaxation on the walls of the cell was the primary disorienting mechanism in our case. With our density of atoms, $\approx 10^{13}$ cm^{-3}, the mean free path was several times greater than the cell diameter, and atom-atom collisions were less important. We found that in order to observe any optical-pumping signal with the radioisotopes, the cell had to be heated, typically to ≈ 500°K. This was accomplished with the use of a small gas burner placed under the cell.

Another important effect associated with the relaxation process is that of the tail of the cell. In order to fill the cell, an entrance is required. It is difficult to seal the cell right at the surface, and usually a tail is left. Unless there is some limitation on the movement of atoms between the tail and the volume of the cell, unorientated atoms in the tail are free to enter the volume of the cell, while the oriented atoms can leave the path of the pumping light beam. In the tail they become disoriented. In the case of a wet cell, that contains a reservoir of mercury, the atoms become disoriented upon condensation. This relaxation process was, in fact, responsible for the early failure of optical-pumping experiments.[33]

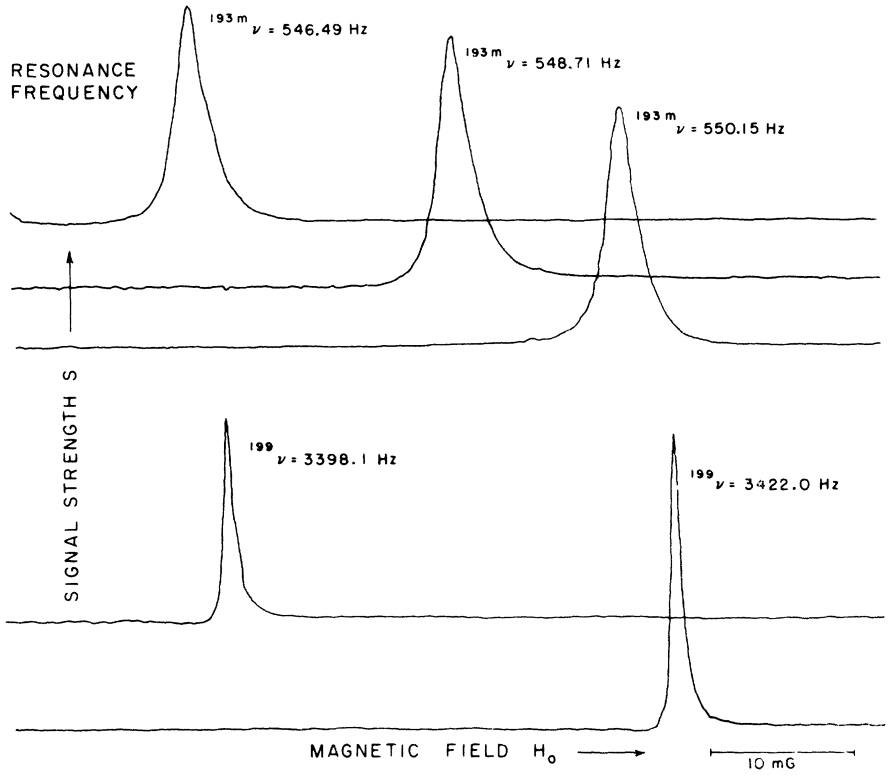

FIG. 8. ^{193m}Hg resonance signals shown with the ^{199}Hg calibration resonances.

The solution of this problem is due to Cagnac.[14] A thin capillary, approximately 1 mm in diam and 10 mm long, is attached to the cell. The cross-sectional area of the capillary is minute compared to the entire area of the cell, and therefore a very small fraction of the oriented atoms can leave the cell. The capillary does not interfere with the process of filling the cell. The placement of the capillary tube is clearly seen in the photograph of the optical-pumping cell (Fig. 4). Walter,[15] worked with a constriction at the base of the cell, but did not use a capillary tube. This may have been a contributing factor to his ability to pump the spin-$\frac{1}{2}$ isotope ^{197}Hg but not its spin-$\frac{13}{2}$ isomer, for which there are more relaxation mechanisms. However, a more likely reason for his difficulties may have been lack of intensity of the pumping light.

B. Procedure and Results

The optical-pumping NMR signal of ^{199}Hg allowed the calibration of the magnetic field H_0, since its magnetic moment had been determined previously with great accuracy by Cagnac.[14] The magnetic field was swept over a constant range and reference points were established by obtaining two ^{199}Hg resonance signals, one at either end of the sweep range. The constancy of the magnetic field sweep range was ascertained by observing the stability of the ^{199}Hg NMR peak upon successive sweeps. The oscillator was then set at the approximate frequency of the radioisotope resonance, and the field was again swept over the resonance range. In this manner a ratio of the resonance frequencies of the radioisotopes and ^{199}Hg could be obtained. In turn, this allowed a determination of the nuclear g-value ratio and the magnetic moment of the radioisotope. Thus $\nu/^{199}\nu = |g/^{199}g|$, and $|\mu| = |g/^{199}g| \times (I/^{199}I) \times |^{199}\mu|$.

TABLE II. ^{193}Hg, ^{193m}Hg, ^{195m}Hg, and ^{197m}Hg results. The errors quoted for the g-value ratios represent three standard deviations of the measurements shown in Table VI. The magnetic moments were calculated with the use of Cagnac's result (Ref. 14), $^{199}\mu = 0.497\,865(6)\mu_N$. The differential hfs anomalies, $\Delta \approx \epsilon - \epsilon_{199}$, with respect to ^{199}Hg, were calculated from Eq. (II.4) with the use of the A values listed in Table III. The single s-electron hfs anomaly is $\Delta_s \approx 1.13\Delta(^3P_1)$.

Mercury isotopes	$\lvert g/^{199}g\rvert$	μ (μ_N)	$\Delta^{199}(6s6p\ ^3P_1)$
193	0.413 52(12)	−0.617 63(18)	0.0054(27)
193m	0.160 93(5)	−1.0416(3)	0.0108(3)
195m	0.158 83(3)	−1.0280(2)	0.0106(2)
197m	0.156 23(4)	−1.0112(3)	0.0105(6)

Recordings of some experimental resonance signals are shown in Figs. 5–8.

1. MEASUREMENTS

The results of the individual nuclear g-factor ratio measurements are presented in Appendix II. The averages and the calculated errors are given in Table II. In column 3, Table II, we give the corresponding values of the magnetic moments, without diamagnetic correction. In calculating these, we used the value[14] $^{199}\mu = 0.497\,865(6)\mu_N$. The signs were obtained from previous optical-spectroscopic and level-crossing hfs measurements.[18,34,35] In Table III, we list the previously measured A values for the pertinent isotopes. These allow, with the use of Eq. (II.4), the calculation of the hfs anomalies given in Table II. The large uncertainty in the value $^{193}\Delta^{199}$ arises from the lack of precision of the measurement of the magnetic dipole hfs interaction constant of ^{193}Hg.

The comparison of the measured hfs anomalies with theory is usually through a_s, the contribution to the magnetic dipole hfs interaction constant $A(6s6p\ ^3P_1)$ of the s electron. The value Δ_s can be obtained from $\Delta(^3P_1)$ as shown by McDermott and Lichten[36] and by Stager.[37] With the use of the intermediate coupling constants that we have summarized recently,[38] the appropriate relativistic corrections, calculable from the results of Casimir,[39] and the hfs measurements in the $6s6p\ ^3P_2$ state of mercury,[36] we calculate $\Delta_s \approx (1.13\Delta(^3P_1)$. As was done by Stager,[37] this result neglects the hfs anomaly of the $p_{1/2}$ electron,[3] $[\Delta(p_{1/2})/\Delta_s \approx 0.2]$, and its contribution ≈ 0.02 to the above $\Delta_s/\Delta(^3P_1)$ ratio, as well as the contribution of the off-diagonal $a_{1/2,3/2}$ term.

2. DISCUSSION

The nuclear magnetic moments had already been determined to within a few percent (limited by the lack of knowledge of the hfs anomalies) from the

TABLE III. Magnetic dipole hfs interaction constants of mercury isotopes used in calculating the hfs anomalies in Table II.

Mercury isotopes	A (MHz)	Reference
193	−6133(15)	35
193m	−2399.69(6)	a
195m	−2368.04(8)	a
197m	−2328.89(84)	b
199	147 52.37(1)	37

[a] W. W. Smith, Phys. Rev. 137, A330 (1965).
[b] H. R. Hirsch, J. Opt. Soc. Am. 51, 1192 (1961); C. Brot, J. Phys. Radium 22, 412 (1961).

previously measured A values. The direct, precision measurements of μ permit us now further to obtain Δ, a measure of the distribution of nuclear magnetization.

In Fig. 9 we show a plot of the differential hfs anomalies of all measured mercury isotopes. These include the present results, those previously summarized by us,[18] and our recent measurements of ^{203}Hg.[26,38] The anomalies for those isotopes the odd neutron of which occupies the same shell-model state have been connected with dashed lines to show the variation of Δ with neutron number. The dependence of the hfs anomalies on angular momentum is apparent. Since ^{199}Hg, with its odd $3p_{1/2}$ neutron, is taken as a reference, it is easily understood that the remaining isotopes with an odd $3p_{1/2}$ neutron display small differential hfs anomalies because the zero-order contribution to their nuclear magnetization is essentially identical, i.e., that of the odd particle. The remaining three sets of isotopes show that the larger the difference in angular momentum, the larger is the difference of the effect on the hfs caused by the departure from point magnetization, and hence Δ. This is consistent with the observations[3] that the largest values of Δ occur for pairs of odd-A isotopes where the addition of a neutron pair leads to a spin change. For a given angular momentum state the variation of Δ with neutron number reflects the differing nucleon excitations that one must consider when one includes configurations admixtures to the zero-order shell-model states.[3] We consider this in more detail in Sec. 2a below.

a. Nuclear Configuration-Mixing Theory

The nuclear configuration-mixing theory (CMT), as formulated by Noya, Arima, and Horie,[40] was used to calculate the nuclear magnetic moments and, in our formalism,[3] the hfs anomalies of all the mercury isotopes for which experimental determinations of these quantities have been made. The theory extends the basic shell model by allowing the residual nucleon interactions, represented by a δ-function force, to break up nucleon pairs, initially coupled to zero angular momentum. These nucleons can then contribute to the nuclear moments. The excited admixed configurations that contribute to the magnetic dipole moment are limited by the selection rule $\Delta l = 0$, $\Delta j = \pm 1$, for the protons and neutrons. For the hfs anomaly, the operator also admits contributions from configurations that differ by 2 in nucleon orbital angular momentum. The specification of the strength of the nucleon interaction (we used $C = 30$ MeV in Ref. 40) and of the ground-state proton and neutron configurations that, through nucleon excitations, contribute to μ and ϵ allows the calculation of the departures from the single-particle shell-model values. For the magnetic dipole moments, the latter are simply the Schmidt limits. In assigning the plausible ground-state configurations, the competition between single-particle and pairing energies is considered. The latter generally favors the filling of pairs in the higher-angular-momentum orbits.

Mercury has 80 protons, two less than the closed

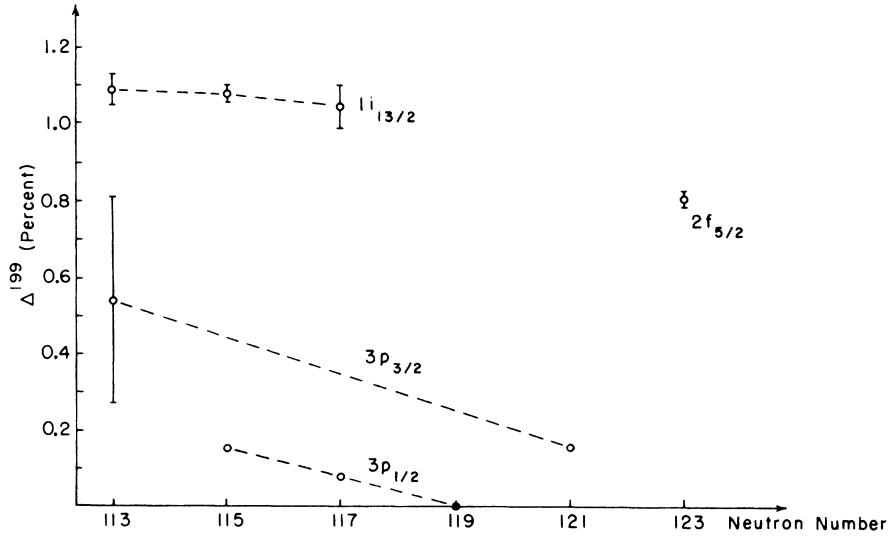

FIG. 9. Systematics of differential hfs anomalies ${}^{A}\Delta^{199} \approx [({}^{A}A)({}^{199}g)/({}^{199}A)({}^{A}g)] - 1$ of mercury isotopes. The superscripts A denote the mass number.

shell of 82. The missing proton pair is expected to be taken from the $3s_{1/2}$ level which lies highest in this shell. Thus the contributing proton configuration used in the calculations is $(1h_{11/2})^{12}$.

The assignment of the neutron configurations is more ambiguous. After the closed shell at 82, the neutrons in the low-lying levels of the next shell fill the $(1h_{9/2})$ and $(2f_{7/2})$ orbits, bringing the total number of neutrons to 100. The remaining four energy levels of this shell lie extremely close together. For ^{193}Hg the $3p_{3/2}$, $3p_{1/2}$, $2f_{5/2}$, and $1i_{13/2}$ levels are all within 0.14 MeV. Since pairing energies are generally larger than this, neutron pairs are expected to fill the higher-angular-momentum states first. The odd neutrons, on the other hand, are expected to be found in the lower-angular-momentum states. This is evidenced by the spins of the ground states of the odd-mass-number isotopes.

In order to obtain reasonable results for both the nuclear magnetic moments and the hfs anomalies of the two spin-$\frac{3}{2}$ isotopes, it was necessary to combine the results of the CMT calculations for two different zero-order configurations. These differed from each other by the transfer of a pair of neutrons from the $3p_{3/2}$ to the $3p_{1/2}$ level. The closeness of these energy levels is predicted by the shell model and is manifested by the change of spin from $\frac{3}{2}$ for ^{193}Hg, to $\frac{1}{2}$ for the isotopes 195, 197, and 199, and back to $\frac{3}{2}$ for ^{201}Hg. A similar procedure was found to improve the results for the spin-$\frac{13}{2}$ isomers $193m$ and $197m$.

Since in our calculations[3] we obtain Δ_s rather than $\Delta(^3P_1)$, we must divide the theoretical result by 1.13, as discussed in Sec. 2 above, in order to make comparisons with experiment.

b. *Details of Calculations*

Spin-$\frac{1}{2}$ isotopes. CMT does not lead, if a δ-function force is used, to corrections to the zero-order values of the magnetic dipole moment and hfs anomaly for nuclei for which the odd neutron is in a $p_{1/2}$ state. In fact, the effects of configuration mixing are small for these nuclei. This is shown by the experimental values of the nuclear magnetic moments of the odd-$p_{1/2}$ nuclei ^{195}Hg, ^{197}Hg, and ^{199}Hg, which lie close to the Schmidt value. It may be reasonable to assume that the zero-order values of the anomalies should also be close to their experimental values. The results for both μ and ϵ in this case, are therefore independent of the chosen neutron configuration.

Spin-$\frac{3}{2}$ isotopes. ^{193}Hg and ^{201}Hg are the spin-$\frac{3}{2}$ nuclei. For ^{193}Hg the configuration

$$(3p_{3/2})^3(3p_{1/2})^0(2f_{5/2})^4(1i_{13/2})^6$$

yields values for the magnetic moment and the anomaly $\epsilon(^3P_1)$ of $-0.473\mu_N$ and -1.941%, respectively, while the configuration

$$(3p_{3/2})^1(3p_{1/2})^2(2f_{5/2})^4(1i_{13/2})^6$$

yields values of $-1.428\mu_N$ and -4.494%. It is possible to obtain reasonable results for both the magnetic dipole moment and the hfs anomaly by taking a combination of these two configurations. The coefficients for this combination are 0.6 for the former configuration and 0.4 for the latter.

A similar procedure is followed for ^{201}Hg where

$$(3p_{3/2})^3(3p_{1/2})^0(2f_{5/2})^4(1i_{13/2})^{14}$$

and

$$(3p_{3/2})^1(3p_{1/2})^2(2f_{1/2})^4(1i_{13/2})^{14}$$

result in magnetic moments $-0.232\mu_N$ and $-1.190\mu_N$, and anomalies -1.409 and -4.241, respectively. A choice of 0.4 for the first and 0.6 for the second configuration yields optimum results for both the anomaly and the magnetic moment.

Spin-$\frac{5}{2}$ isotopes. The magnetic moment of the 3.3-nsec state of ^{199}Hg has been measured by Grodzins, Bauer, and Wilson[41] using γ-ray angular correlation techniques. The configuration $(3p_{3/2})^2(3p_{1/2})^0(2f_{5/2})^5(1i_{13/2})^{12}$ yields a magnetic moment in good agreement with the experimental determination. The configuration

$$(3p_{3/2})^4(3p_{1/2})^0(2f_{5/2})^5(1i_{13/2})^{14}$$

chosen for ^{203}Hg yields good results for both μ and ϵ.

Spin-$\frac{13}{2}$ isotopes. It was found that several possible configuration yielded reasonable results for both the magnetic moments and hfs anomalies of the nuclear isomers. For ^{193m}Hg the configurations

$$(3p_{3/2})^2(3p_{1/2})^0(2f_{5/2})^4(1i_{13/2})^7$$

and

$$(3p_{3/2})^2(3p_{1/2})^0(2f_{5/2})^2(1i_{13/2})^9$$

result in magnetic moments of -1.126 and $-0.880\mu_N$, respectively, and in anomalies of -2.91 and -2.51%. If we mix these two configurations in order to obtain a better accord in the magnetic-moment values, the anomaly result is also improved. The mixing coefficients used were 0.6 and 0.4, respectively.

The ^{195m}Hg configuration

$$(3p_{3/2})^2(3p_{1/2})^0(2f_{5/2})^4(1i_{13/2})^9$$

gave good results for μ and ϵ without a further admixture.

For ^{197m}Hg the configurations

$(3p_{3/2})^2(3p_{1/2})^0(2f_{5/2})^4(1i_{13/2})^{11}$

gave $\mu = 0.883\mu_N$ and $\epsilon(^3P_1) = -2.550\%$. It was mixed in an equal amount with the configuration $(3p_{3/2})^0(3p_{1/2})^0(2f_{5/2})^6(1i_{13/2})^{11}$, which gives $\mu = -1.108\mu_N$ and $\epsilon(^3P_1) = -3.045\%$.

c. Conclusion

The results of these calculations are summarized in Table IV for the magnetic moments, and in Table V for the hfs anomalies. It is seen that with the use of CMT we can account reasonably well for both the magnetic dipole moments and the hfs anomalies, except for the spin-$\frac{3}{2}$ isotopes. Here the numerical agreement is not as good, though the signs are correct, as are the relative magnitudes of the moments and anomalies for ^{193}Hg and ^{201}Hg.

There are several trends apparent from the plot (Fig. 9) of the experimentally determined anomalies. For isotopes of a given spin, the anomaly becomes more negative with increasing neutron number. This may be expected qualitatively, since the hfs anomalies result from the difference in interaction energies between nuclei of different distributed nuclear magnetization. Greater numbers of neutrons spread the magnetization over a larger volume and can thereby reduce the interaction energy with the electron at the origin.

The absolute values of the anomalies ϵ (which are all negative in our cases) are larger for the lower-spin nuclei. The CMT equations predict this: The value of the calculated anomaly is inversely proportional to the magnitude of the nuclear magnetic moment. As can be seen in Table IV, the lower-spin nuclei have progressively smaller magnetic moments than those of the high-spin nuclei, and have, consequently, larger magnitudes of the anomalies ϵ.

TABLE IV. Comparison with experiment of single-particle (sp) (Schmidt limit) and configuration-mixing theory (CMT) calculations of the nuclear magnetic moments of mercury isotopes.

Isotope	μ_{sp} (Schmidt) (μ_N)	μ (CMT) (μ_N)	μ (exp.) (μ_N)
193	−1.913	−0.855	−0.617 63(18)
193*m*	−1.913	−1.028	−1.0416(3)
195	0.638	0.638	0.532 892(33)
195*m*	−1.913	−1.004	−1.0280(2)
197	0.638	0.638	0.519 014(14)
197*m*	−1.913	−0.996	−1.0112(3)
199	0.638	0.638	0.497 865(6)
199*	1.366	1.013	1.03(8)
201	−1.913	−0.817	−0.551 344(9)
203	1.366	0.894	0.835 49(13)

ACKNOWLEDGMENTS

We are grateful to Professor O. Redi, Princeton University, for valuable discussions and help. We also wish to thank D. Shernoff for technical assistance in the making of light sources and cells, and Dr. A. Koehler and the staff of the Harvard University cyclotron for the irradiations.

APPENDIX I

Optical-Pumping Signal

We outline the calculation of the optical-pumping signal in which we use the density-matrix formalism as presented by Carver and Partridge.[27] This is done most simply for a spin-$\frac{1}{2}$ system. It has been developed further for our geometry by King.[32] The possibility of the generalization of the results to higher angular momenta has been noted by Carver and Partridge.[27]

The signal S is obtained from the expectation value of an appropriate monitoring operator M for the emission of electric dipole radiation. This is evaluated with the use of the density matrix ρ. Letting $\vec{g}$ be the polarization vector and $-e\vec{r}$ the electric-dipole-moment operator, we have[24]

TABLE V. Comparison with experiment of configuration-mixing theory (CMT) calculations of the hfs anomalies, ϵ, of mercury isotopes. The differential hfs anomaly in the $6s6p\ ^3P_1$ state with respect to ^{199}Hg, $^A\Delta^{199} \approx \epsilon_A - \epsilon_{199}$, is the experimentally measured value. The calculated values for ϵ are for a single s electron. We used the relation (Sec. IV B 2) $\Delta_s \approx 1.13\Delta(^3P_1)$.

Isotope A	Spin	CMT $\epsilon(^3P_1)$ (%)	CMT $\epsilon - \epsilon_{199}$ (%)	$^A\Delta^{199}$ exp. (%)
195	$\frac{1}{2}$	−3.64	0.24	0.147(9)
197	$\frac{1}{2}$	−3.72	0.16	0.077(4)
199	$\frac{1}{2}$	−3.88	0.0	0.0
193	$\frac{3}{2}$	−2.96	0.92	0.54(27)
201	$\frac{3}{2}$	−3.11	0.77	0.163(2)
203	$\frac{5}{2}$	−3.29	0.59	0.81(2)
193*m*	$\frac{13}{2}$	−2.75	1.13	1.08(3)
195*m*	$\frac{13}{2}$	−2.72	1.16	1.06(2)
197*m*	$\frac{13}{2}$	−2.80	1.08	1.05(6)

$$M_{m'm} = C\sum_{\mu}\langle m|\vec{g}\cdot\vec{r}|\mu\rangle^{*}\langle m'|\vec{g}\cdot\vec{r}|\mu\rangle$$
$$= C\sum_{\mu}\langle\mu|\vec{g}^{*}\cdot\vec{r}^{\dagger}|m\rangle\langle m'|\vec{g}\cdot\vec{r}|\mu\rangle$$
$$= C\sum_{\mu}\langle m'|\vec{g}\cdot\vec{r}|\mu\rangle\langle\mu|\vec{g}^{*}\cdot\vec{r}|m\rangle\ , \qquad (A.1)$$

where C is a constant. We have used the fact that $\vec{r}$ is a Hermitian vector operator, while $\vec{g}\cdot\vec{r}$ is not. The magnetic quantum numbers in the excited and ground states are denoted by m and μ, respectively. We have then

$$\langle M\rangle = \mathrm{Tr}(\rho M) = \sum_{mm'}\rho_{mm'}(t)M_{m'm}\ . \qquad (A.2)$$

The density matrix, for the conditions of magnetic fields H_0 and H_1 given in Sec. III, is calculated[27] for $J=\frac{1}{2}$:

$$\rho(t) = \frac{W}{\Gamma}\begin{vmatrix} 1-\frac{1}{2}P & \frac{1}{2}(\chi'+i\chi'')e^{-i\omega t} \\ \frac{1}{2}(\chi'-i\chi'')e^{i\omega t} & \frac{1}{2}P \end{vmatrix}, \qquad (A.3)$$

where $P\equiv(\gamma H_1)^2/[\Gamma^2(\omega_0-\omega)^2+(\gamma H_1)^2]$, and W is determined by the optical-pumping rate

$$\rho(t) = W\rho^0\ . \qquad (A.4)$$

If we assume excitation by circularly polarized light with negative helicity, we have

$$\rho^0 = \begin{vmatrix} 1 & 0 \\ 0 & 0 \end{vmatrix}\ . \qquad (A.5)$$

This was used in obtaining (A.3), and is the experimental condition for both the Dehmelt[11] and Bell and Bloom[13] arrangements. In the former, the detection of the signal is that of circularly polarized light along the z direction. The appropriate polarization vector in (A.1) is thus $\vec{g}=\vec{e}_x+i\vec{e}_y$. In the latter, the modulation is detected in the circularly polarized light of a cross beam along the y direction. For this case $\vec{g}=\vec{e}_x+i\vec{e}_z$. In spherical tensor notation[42]

$$\vec{g}_{\pm1} = \mp(1/\sqrt{2})(\vec{g}_x \pm i\vec{g}_y), \quad \vec{g}_0 = \vec{g}_z,$$
$$\vec{r} = \sum_q (-1)^q r_q^1 \vec{e}_{-q}\ .$$

In this form it is straightforward to calculate the matrix elements required in (A.1) with the use of the Wigner-Eckart theorem (Ref. 42, p. 75). The monitoring operator becomes for this case

$$M = C\times\tfrac{1}{3}\left|\left(\tfrac{1}{2}\middle|\middle|\vec{r}\middle|\middle|\tfrac{1}{2}\right)\right|^2\begin{vmatrix} 1 & i \\ -i & 1 \end{vmatrix}\ . \qquad (A.6)$$

With the use of (A.3) and (A.6) in (A.2) we obtain the result for the signal $S=K(-\chi'\sin\omega t+\chi''\cos\omega t)$. This is the ac part, with frequency ω, of $\langle M\rangle$. The result differs in phase by $\pi/2$ from S given in (III 1), which holds for spins larger than $\frac{1}{2}$. The difference in phase between the two results was observed by noting in an experiment that for the phase setting of the detector that yielded a Lorentz-shaped signal (χ'' term) for the spin-$\frac{1}{2}$ isotope (^{199}Hg), a dispersion-shaped signal (χ' term) was obtained for the isotopes with spin greater than $\frac{1}{2}$ (e.g., ^{193}Hg, $I=\frac{3}{2}$, ^{193m}Hg, $I=\frac{13}{2}$).

With our geometry, i.e., circularly polarized light incident in the yz plane at 45° with respect to H_0, we can write the polarization vector as

$$\vec{e}_x+\frac{i}{\sqrt{2}}(\vec{e}_y+\vec{e}_z) = \tfrac{1}{2}(\vec{e}_x+i\vec{e}_y)+\tfrac{1}{2}(\vec{e}_x+i\vec{e}_z)$$
$$+\frac{i}{2}(\vec{e}_y+\vec{e}_z)(\sqrt{2}-1)\ . \qquad (A.7)$$

The first and second terms on the right-hand side of (A.7) are seen to correspond to the pumping and monitoring beams, respectively, in the Bell and Bloom experiment, but with reduced intensity. Furthermore the last term decreases the degree of orientation. The decrease is seen most simply by considering the effect on ρ^0 of a rotation of the z axis by 45°. We have (Ref. 42, p. 56) $\rho^{0\prime} = d^{1/2}\rho^0(d^{1/2})^{-1}$, where the appropriate rotation matrix (with $\beta=45°$ in our case) is

$$d^{1/2}(\beta) = \begin{vmatrix} \cos\frac{1}{2}\beta & \sin\frac{1}{2}\beta \\ -\sin\frac{1}{2}\beta & \cos\frac{1}{2}\beta \end{vmatrix}\ . \qquad (A.8)$$

The result can be put in the form[32]

$$\rho^{0\prime} = \begin{vmatrix} a-b & 0 \\ 0 & 0 \end{vmatrix} + \begin{vmatrix} b & 0 \\ 0 & b \end{vmatrix} + \begin{vmatrix} 0 & c \\ c & 0 \end{vmatrix}\ . \qquad (A.9)$$

For $\beta=45°$, $a-b=\cos^2(\frac{1}{2}\beta)-\sin^2(\frac{1}{2}\beta)\approx 0.7$. This represents the loss of orientation. The second term does not contribute to the optical-pumping signal, while the third leads to terms [Ref. 27, Eq. (22)] in 2ω to which our detection was not sensitive. For higher angular momenta, we can calculate comparable orientation degradation.

TABLE VI. Data of g-factor-ratio measurements with respect to ^{199}Hg of the radioisotopes ^{193}Hg, ^{193m}Hg, ^{195m}Hg, and ^{197m}Hg. We denote by σ_0 the standard deviation of the average.

	$^{193}\nu/^{199}\nu$	$^{193m}\nu/^{199}\nu$	$^{195m}\nu/^{199}\nu$	$^{197m}\nu/^{199}\nu$
		0.160 99	0.158 85	
		0.161 08	0.158 79	0.156 30
		0.160 91	0.158 86	0.156 30
	0.413 60	0.160 90	0.158 88	0.156 21
	0.413 60	0.160 88	0.158 87	0.156 21
	0.413 40	0.160 85	0.158 78	0.156 21
	0.413 40	0.160 91	0.158 81	0.156 21
	0.413 41	0.160 95	0.158 84	0.156 22
	0.413 45	0.160 93	0.158 83	0.156 23
	0.413 64	0.160 93	0.158 82	0.156 20
	0.413 65	0.160 93	0.158 82	0.156 25
$\langle^A\nu/^{199}\nu\rangle_{\mathrm{av}}$	0.413 519	0.160 933	0.158 832	0.156 234
σ_0	0.000 040	0.000 018	0.000 010	0.000 012

APPENDIX II

Detailed Presentation of Data

In Table VI we present the results of the individual measurements obtained of the g-factor ratios. The standard deviation of the average of these results, σ_0, is equal to $\{\sum_n |\delta x|^2/[n(n-1)]\}^{1/2}$, where n is the total number of measurements and δx is the deviation from the average value of a given measurement. The errors quoted in Table II for these results are $3\sigma_0$. Systematic errors are estimated to be small compared to σ_0. The average values given in Table VI were rounded off suitably in Table II.

---

†Work supported by the National Science Foundation Grant No. GP 15228, in part by the James Arthur Endowment Fund of New York University, and an equipment Grant No. DA-ARO-D-31-124-G763 from the Army Research Office. A report of these results was presented at the meeting of the Division of Nuclear Physics of the American Physical Society, Houston, Texas, 16 October 1970, Abstract DC 9.

*The results of this work are to be submitted by P. A. Moskowitz to the Department of Physics, New York University, in partial fulfillment of the requirements for the degree of Doctor of Philosophy.

‡Present address: Department of Physics, University of Arizona, Tucson, Arizona 85721.

[1]H. H. Stroke, in *Atomic Physics*, edited by B. Bederson, V. W. Cohen, and F. M. J. Pichanick (Plenum Press, Inc., New York, 1969), p. 523.

[2]Nuclear orientation in ^{197m}Hg has also been reported more recently by R. J. Reimann, C. C. Chan, and M. N. McDermott at the meeting of the Division of Electron and Atomic Physics of the American Physical Society, Seattle, Washington, 23 November 1970, Abstract DA 4. We thank Professor McDermott and Dr. Reimann for also communicating to us their success with the other isotopes, including ^{199m}Hg (H. H. Stroke, private communication).

[3]F. Bitter, Phys. Rev. 76, 150 (1949); A. Bohr and V. F. Weisskopf, *ibid.* 77, 94 (1950); H. H. Stroke, R. J. Blin-Stoyle, and V. Jaccarino, *ibid.* 123, 1326 (1961).

[4]E. Fermi and F. Rasetti, Z. Physik 33, 246 (1925).

[5]F. Bitter, Phys. Rev. 76, 833 (1949).

[6]M. H. L. Pryce, Phys. Rev. 77, 136 (1950).

[7]J. Brossel and A. Kastler, Compt. Rend. 229, 1213 (1949).

[8]J. Brossel, P. Sagalyn, and F. Bitter, Phys. Rev. 79, 196, 225 (1950); see also *Francis Bitter, Selected Papers and Commentaries*, edited by T. Erber and C. M. Fowler (The Massachusetts Institute of Technology Press, Cambridge, Massachusetts, 1969), pp. 308, 355.

[9]A. Kastler, J. Phys. Radium 11, 255 (1950).

[10]J. Brossel, A. Kastler, and J. Winter, J. Phys. Radium 13, 668 (1952).

[11]H. G. Dehmelt, Phys. Rev. 105, 1487 (1957).

[12]H. G. Dehmelt, Phys. Rev. 105, 1924 (1957).

[13]W. E. Bell and A. Bloom, Phys. Rev. 107, 1559 (1957).

[14]B. Cagnac, Ph.D. thesis, University of Paris, 1960 (unpublished); Ann. Phys. (Paris) 6, 467 (1961).

[15]W. T. Walter, Bull. Am. Phys. Soc. 7, 295 (1962); Ph.D. thesis, Massachusetts Institute of Technology, Cambridge, Massachusetts, 1962 (unpublished).

[16]H. Kopfermann, *Nuclear Moments* (Academic Press Inc., New York, 1958), Chap. 1.

[17]A. de-Shalit and I. Talmi, *Nuclear Shell Theory* (Academic Press Inc., New York, 1963), p. 180.

[18]W. J. Tomlinson and H. H. Stroke, Nucl. Phys. 60, 614 (1964).

[19]G. Breit and J. E. Rosenthal, Phys. Rev. 41, 459 (1932); H. J. Rosenberg and H. H. Stroke, Bull. Am. Phys. Soc. 14, 84 (1969).

[20]G. H. Fuller and V. W. Cohen, Oak Ridge National Laboratory Report No. ORNL 4591 UC 34 Physics, September, 1970 (unpublished).

[21]C. S. Wu and L. Wilets, Ann. Rev. Nucl. Sci. 19, 527 (1969).

[22]J. F. Waymouth, S. W. Thompson, L. C. Bradley, III, and H. H. Stroke, Massachusetts Institute of Technology, Research Laboratory of Electronics, Quart. Progr. Report 58, 102 (1960).

[23]W. T. Walter and M. J. Stavn, Bull. Am. Phys. Soc. 9, 10 (1964).

[24]C. Cohen-Tannoudji, Ph.D. thesis, University of Paris, 1962 (unpublished); Ann. Phys. (Paris) 7, 423, 469 (1962).

[25]A. Kastler, Science 158, 214 (1967).

[26]R. L. King, C. H. Liu, H. H. Stroke, and O. Redi, Phys. Letters 31B, 567 (1970).

[27]T. R. Carver and R. B. Partridge, Am. J. Phys. 34, 339 (1966).

[28]G. Fulop, C. H. Liu, P. Moskowitz, H. H. Stroke, and O. Redi, Bull. Am. Phys. Soc. 15, 1509 (1970); G. Fulop, Ph.D. thesis, New York University, June 1971 (unpublished).

[29]D. I. Shernoff, Rev. Sci. Instr. 40, 1418 (1969).

[30]N. Poffé, G. Albouy, M. Gusakow, and J. L. Sarrouy, J. Phys. Radium 22, 639 (1961).

[31]N. Poffé, Ph.D. thesis, University of Paris, 1964 (unpublished).

[32]R. L. King, Ph.D. thesis, New York University, February 1970 (unpublished).

[33]H. H. Stroke, in *Francis Bitter, Selected Papers and Commentaries*, edited by T. Erber and C. M. Fowler (The Massachusetts Institute of Technology Press, Cambridge, Massachusetts, 1969), pp. 289, 290.

[34]H. Kleiman, S. P. Davis, and T. Aung, Phys. Letters 13, 212 (1964).

[35]O. Redi and H. H. Stroke, Bull. Am. Phys. Soc. 10, 456 (1965).

[36]M. N. McDermott and W. L. Lichten, Phys. Rev. 119, 134 (1960).

[37]C. V. Stager, Phys. Rev. 132, 275 (1963).

[38]O. Redi and H. H. Stroke, Phys. Rev. A 2, 1135 (1970).

[39]H. B. G. Casimir, *On the Interaction Between Atomic Nuclei and Electrons* (W. H. Freeman & Company, San Francisco, California, 1963), p. 54.

[40]H. Noya, A. Arima, and H. Horie, Progr. Theoret. Phys. (Kyoto) Suppl. 8, 33 (1958).

[41]L. Grodzins, R. W. Bauer, and H. H. Wilson, Phys. Rev. 124, 1897 (1961).

[42]A. R. Edmonds, *Angular Momentum in Quantum Mechanics* (Princeton University Press, Princeton, New Jersey, 1957), pp. 69, 82.

FIG. 4. Photograph of optical-pumping cell, and of spherical electrodeless lamps.